

# Particle Acceleration and the Formation of Relativistic Outflows in Viscous Accretion Disks with Shocks

Peter A. Becker,<sup>1</sup> Santabrata Das,<sup>2</sup> and Truong Le<sup>3</sup>

## ABSTRACT

In this Letter, we present a new self-consistent theory for the production of the relativistic outflows observed from radio-loud black hole candidates and active galaxies as a result of particle acceleration in hot, viscous accretion disks containing standing, centrifugally-supported isothermal shocks. This is the first work to obtain the structure of such disks for a relatively large value of the Shakura-Sunyaev viscosity parameter ( $\alpha = 0.1$ ), and to consider the implications of the shock for the acceleration of relativistic particles in viscous disks. In our approach, the hydrodynamics and the particle acceleration are coupled and the solutions are obtained self-consistently based on a rigorous mathematical method. We find that particle acceleration in the vicinity of the shock can provide enough energy to power the observed relativistic jet in M87.

*Subject headings:* accretion, accretion disks — hydrodynamics — black hole physics — galaxies: jets

## 1. INTRODUCTION

It has recently been established that the acceleration of relativistic particles at a standing shock in an advection-dominated accretion flow (ADAF) can power the outflows frequently observed from radio-loud active galactic nuclei (AGNs) and galactic black-hole candidates (Le & Becker 2004, 2005, 2007). Radio-loud AGNs are thought to contain supermassive central

---

<sup>1</sup>College of Science, George Mason University, Fairfax, VA 22030-4444; pbecker@gmu.edu

<sup>2</sup>Astrophysical Research Center, Sejong University, Seoul 143-747, Korea; sbdas@canopus.cnu.ac.kr

<sup>3</sup>E. O. Hulburt Center for Space Research, Naval Research Laboratory, Washington, DC 20375; tle@ssd5.nrl.navy.mil

black holes surrounded by hot, two-temperature ADAFs with significantly sub-Eddington accretion rates. In these disks, the ion temperature  $T_i \sim 10^{12}$  K greatly exceeds the electron temperature  $T_e \sim 10^{10}$  K (e.g., Narayan, Kato, & Honma 1997; Becker & Le 2003). The observed correlation between high radio luminosities and the presence of the outflows suggests that hot ADAF disks are able to efficiently accelerate the relativistic particles powering the jets. In fact, such disks are ideal sites for first-order Fermi acceleration at shocks because the gas is tenuous, and therefore a significant fraction of the accelerated particles are able to avoid thermalization and escape from the disk. Although the work of Le & Becker (2004, 2005, 2007) was the first to establish a direct connection between the structure of the disk/jet system and a specific microphysical particle acceleration mechanism, their model was only applicable to fully inviscid (adiabatic) disks. In this Letter, we generalize their model to include viscous dissipation.

## 2. DYNAMICAL MODEL

The dynamical structure of the accretion disks considered here is based on the viscous inflow model studied by Narayan et. al (1997), Lu, Gu, & Yuan (1999), Gu & Lu (2001), and Becker & Le (2003), with the addition of an isothermal shock. In the one-dimensional, vertically-integrated, steady state ADAF scenario under consideration here, the accretion rate  $\dot{M}$  and the angular momentum transport rate  $\dot{J}$  are conserved, where

$$\dot{M} \equiv 4\pi r H \rho u, \quad \dot{J} \equiv \dot{M} \ell - \mathcal{G}, \quad (1)$$

with  $\rho$  denoting the mass density,  $u$  the radial velocity (defined to be positive for inflow),  $H$  the disk half-thickness,  $\ell = r^2 \Omega$  the specific angular momentum,  $\Omega$  the angular velocity, and  $\mathcal{G}$  the torque. The vertical hydrostatic structure of the disk is described by the usual relations

$$H(r) = \frac{r^2 a}{\ell_K}, \quad a^2(r) = \frac{P}{\rho}, \quad (2)$$

where  $a$  denotes the isothermal sound speed, and  $\ell_K$  represents the Keplerian angular momentum per unit mass for matter orbiting in the pseudo-Newtonian potential  $\Phi$ , given by (Paczynski & Wiita 1980)

$$\ell_K^2(r) \equiv \frac{GM r^3}{(r - r_s)^2} = r^3 \frac{d\Phi}{dr}, \quad (3)$$

with  $r_s \equiv 2GM/c^2$  denoting the Schwarzschild radius for a black hole of mass  $M$ . The energy transport rate

$$\dot{E} = -\mathcal{G} \frac{\ell}{r^2} + \dot{M} \left( \frac{1}{2} \frac{\ell^2}{r^2} + \frac{1}{2} u^2 + \frac{P+U}{\rho} + \Phi \right), \quad (4)$$

is also conserved (except at the shock, if one is present), where  $U$  is the internal energy density,  $P$  is the gas pressure, and all quantities represent vertical averages. We assume that the ratio of specific heats,  $\gamma \equiv (U + P)/U$ , remains constant throughout the flow. Note that the transport rates  $\dot{M}$ ,  $\dot{J}$ , and  $\dot{E}$  are all defined to be positive for inflow.

In a steady state, the comoving radial acceleration rate in the frame of the accreting gas is expressed by

$$\frac{Du}{Dt} \equiv -u \frac{du}{dr} = \frac{1}{\rho} \frac{dP}{dr} + \frac{\ell_K^2 - \ell^2}{r^3}, \quad (5)$$

and the torque  $\mathcal{G}$  is related to the gradient of the angular specific momentum  $\ell$  via (e.g., Frank, King, & Raine 1985)

$$\mathcal{G} = -4\pi r H \rho \nu \left( \frac{d\ell}{dr} - \frac{2\ell}{r} \right), \quad \nu = \frac{\alpha r^2 a^2}{\ell_K}, \quad (6)$$

where  $\nu$  is the kinematic viscosity, computed using the standard Shakura-Sunyaev (1973) prescription, with constant  $\alpha$ . Away from the shock location, the variation of the internal energy density is governed by viscous dissipation and adiabatic compression, and the comoving rate of change of  $U$  is therefore given by (e.g., Becker & Le 2003)

$$\frac{DU}{Dt} \equiv -u \frac{dU}{dr} = -\gamma \frac{U}{\rho} u \frac{d\rho}{dr} + \frac{\rho\nu}{r^2} \left( \frac{d\ell}{dr} - \frac{2\ell}{r} \right)^2. \quad (7)$$

By combining various relations, one can obtain the differential dynamical equation (e.g., Narayan et. al 1997)

$$\left( \frac{u^2}{a^2} - \frac{2\gamma}{\gamma+1} \right) \frac{d \ln u}{dr} = \frac{\ell^2 - \ell_K^2}{a^2 r^3} + \frac{2\gamma}{\gamma+1} \left( \frac{3}{r} - \frac{d \ln \ell_K}{dr} \right) + \left( \frac{\gamma-1}{\gamma+1} \right) \frac{u \ell_K (\ell - j)^2}{\alpha a^4 r^4}, \quad (8)$$

where  $j \equiv \dot{J}/\dot{M}$ . This expression is supplemented by the differential conservation equation for the specific angular momentum,

$$\frac{d\ell}{dr} = \frac{2\ell}{r} - \frac{u \ell_K (\ell - j)}{\alpha r^2 a^2}, \quad (9)$$

obtained by utilizing equations (1) and (6). Dynamical solutions are computed by simultaneously integrating equations (8) and (9). In order to ensure the stability of the calculations, the integrations are performed in the outward direction, starting with initial values near the event horizon computed using the boundary conditions derived by Becker & Le (2003).

The resulting disk/shock model depends on several parameters, namely the energy transport rate per unit mass,  $\epsilon \equiv \dot{E}/\dot{M}$ , the angular momentum transport rate,  $j \equiv \dot{J}/\dot{M}$ , the ratio of specific heats,  $\gamma$ , and the viscosity parameter,  $\alpha$ . The value of  $\epsilon$  is constant in ADAF

disks except at the shock location. When a shock is present, we use the subscripts “-” and “+” to refer to quantities measured just upstream and just downstream from the shock, respectively. Critical points occur where the left- and right-hand sides of equation (8) vanish simultaneously. The flow must pass through at least one critical point before crossing the event horizon since general relativity requires supersonic inflow at the horizon. If the flow is smooth (shock-free), then the gas passes through only one critical point, located at radius  $r = r_c$ . If a shock is present in the flow, then the gas passes through one critical point in the pre-shock region at  $r = r_c^{\text{out}}$ , and through another in the post-shock region at  $r = r_c^{\text{in}}$  (Abramowicz & Chakrabarti 1990).

The isothermal shock radius,  $r_*$ , must be determined self-consistently by satisfying the velocity and energy jump conditions (Chakrabarti 1989)

$$\frac{u_+}{u_-} = \frac{1}{\mathcal{M}_-^2}, \quad \Delta\epsilon \equiv \epsilon_+ - \epsilon_- = \frac{u_+^2 - u_-^2}{2}, \quad (10)$$

where  $\mathcal{M}_- \equiv u_-/a_-$  is the upstream Mach number at the shock location. Note that the velocity jump condition we employ is slightly different from the one utilized by Le & Becker (2005) because those authors defined the Mach number in terms of the adiabatic sound speed rather than the isothermal sound speed used here. Due to the escape of energy at the isothermal shock location, the energy transport rate  $\epsilon$  drops from the upstream value  $\epsilon_-$  to the downstream value  $\epsilon_+$ , and consequently  $\Delta\epsilon < 0$ . The power lost from the disk at the isothermal shock is related to the observed jet kinetic luminosity,  $L_{\text{jet}}$ , via

$$L_{\text{jet}} = -\dot{M} \Delta\epsilon, \quad (11)$$

where  $\dot{M}$  is the accretion rate computed using the observed total energy output for a specific source, and the negative sign appears because  $\Delta\epsilon < 0$ .

For given observational values of  $M$ ,  $\dot{M}$ , and  $L_{\text{jet}}$ , the process of determining the structure for a disk containing an isothermal shock begins with the selection of provisional values for the energy inflow rate  $\epsilon_-$  and the angular momentum inflow rate  $j$ . Next we numerically integrate equations (8) and (9), starting from a location near the horizon and working outward towards the inner critical point. Once a solution is established that passes smoothly through the inner critical point, the next step is to determine the shock location  $r_*$  by ensuring that the shock jump conditions (eqs. [10]) are satisfied. However, if the resulting value of  $\Delta\epsilon$  is not consistent with equation (11), then the values of  $\epsilon_-$  and  $j$  are adjusted and the procedure is repeated starting with the integration from the horizon. When this step is successfully completed, the integration is continued from the upstream side of the shock outward toward the outer critical point. If the flow does not pass smoothly through the outer critical point, then the values of  $\epsilon_-$  and  $j$  are modified and the procedure is repeated

starting from the horizon. The end result is a unique set of values for  $\epsilon_-$  and  $j$ , along with the associated global solution for the disk/shock structure.

### 3. PARTICLE TRANSPORT EQUATION

In a steady-state situation, the Green's function,  $f_G(E, r)$ , representing the particle distribution resulting from the continual injection of monoenergetic seed particles with energy  $E_0$  from a source located at the shock radius  $r_*$  satisfies the vertically-integrated transport equation (Le & Becker 2005, 2007)

$$\begin{aligned}
 -Hu \frac{\partial f_G}{\partial r} &= -\frac{1}{3r} \frac{d}{dr}(rHu) E \frac{\partial f_G}{\partial E} + \frac{1}{r} \frac{\partial}{\partial r} \left( rH\kappa \frac{\partial f_G}{\partial r} \right) \\
 &+ \frac{\dot{N}_0 \delta(E - E_0) \delta(r - r_*)}{(4\pi E_0)^2 r_*} - A_0 c H_* \delta(r - r_*) f_G, \quad (12)
 \end{aligned}$$

where  $H_*$  denotes the disk half-thickness at the shock location,  $\kappa$  is the spatial diffusion coefficient,  $\dot{N}_0$  denotes the particle injection rate,  $c$  is the speed of light, and  $A_0$  is a parameter that describes the rate of particle escape through the upper and lower surfaces of the disk. The left-hand side of equation (12) represents the co-moving (advective) time derivative and the terms on the right-hand side describe first-order Fermi acceleration, spatial diffusion, the particle source, and the escape of particles from the disk, respectively. The relativistic particle number and energy densities associated with the Green's function are given by  $n(r) = \int_0^\infty 4\pi E^2 f_G dE$  and  $U(r) = \int_0^\infty 4\pi E^3 f_G dE$ , respectively. Although the Fermi acceleration of the particles is concentrated at the shock, the rest of the disk also contributes to the particle acceleration because of the general convergence of the MHD waves in the accretion flow.

After the velocity profile has been determined, we can compute the Green's function describing the energy and space distribution of the accelerated relativistic particles inside the disk by solving equation (12). We set the injection energy using  $E_0 = 0.002$  ergs, which corresponds to an injected Lorentz factor  $\Gamma_0 \equiv E_0/(m_p c^2) \sim 1.3$ , where  $m_p$  is the proton mass. The speed of the injected particles,  $v_0 = c(1 - \Gamma_0^{-2})^{1/2}$ , is about three to four times higher than the mean ion thermal velocity at the shock location. The seed particles are picked up from the high-energy tail of the Maxwellian distribution for the thermal ions. The particle injection rate  $\dot{N}_0$  is computed using the energy conservation condition (cf. eq. [11])

$$\dot{N}_0 E_0 = -\dot{M} \Delta\epsilon = L_{\text{jet}}. \quad (13)$$

This self-consistency relation ensures that the energy injection rate for the seed particles is equal to the energy loss rate for the background gas at the isothermal shock location.

To close the system, we specify the radial variation of the spatial diffusion coefficient  $\kappa$  by following Le & Becker (2004, 2005, 2007), who adopted the general form

$$\kappa(r) = \kappa_0 u(r) r_s \left( \frac{r}{r_s} - 1 \right)^2, \quad (14)$$

where  $\kappa_0$  is a dimensionless positive constant. The value of  $\kappa_0$  is determined self-consistently using the energy conservation relation  $L_{\text{jet}} = L_{\text{esc}}$ , where the power in the escaping particles,  $L_{\text{esc}}$ , is computed using  $L_{\text{esc}} = \dot{N}_{\text{esc}} E_*$ , with  $\dot{N}_{\text{esc}}$  denoting the escape rate for the relativistic particles diffusing out of the disk at the shock radius  $r_*$  with mean energy  $E_* = U(r_*)/n(r_*)$ . The spatial diffusion coefficient  $\kappa$  is related to the magnetic mean free path via the usual expression  $\kappa = c \lambda_{\text{mag}}/3$ , where  $\lambda_{\text{mag}}$  denotes the coherence length of the magnetic field. Analysis of the three-dimensional random walk of the escaping particles then yields for the escape parameter  $A_0$  the result (Le & Becker 2005)  $A_0 = (3\kappa_*)^2/(cH_*)^2$ , where  $\kappa_* \equiv (\kappa_- + \kappa_+)/2$ .

For values of the particle energy  $E > E_0$ , the source term in equation (12) vanishes and the remaining equation is separable in energy and space using the functions

$$f_n(E, r) = \left( \frac{E}{E_0} \right)^{-\lambda_n} \varphi_n(r), \quad (15)$$

where  $\lambda_n$  are the eigenvalues, and the spatial eigenfunctions  $\varphi_n(r)$  satisfy the second-order ordinary differential equation

$$-Hu \frac{d\varphi_n}{dr} = \frac{\lambda_n}{3r} \frac{d}{dr} (rHu) \varphi_n + \frac{1}{r} \frac{d}{dr} \left( rH\kappa \frac{d\varphi_n}{dr} \right) - A_0 c H_* \delta(r - r_*) \varphi_n. \quad (16)$$

The eigenvalues  $\lambda_n$  are determined by applying suitable boundary conditions to the spatial eigenfunctions, as discussed by Le & Becker(2007). The eigenvalues  $\lambda_n$  and eigenfunctions  $\varphi_n(r)$  can be determined numerically by computing  $H(r)$  and  $\kappa(r)$  using equations (2) and (14), respectively, once a numerical solution for the inflow speed  $u(r)$  has been obtained (Le & Becker 2005).

We can establish several useful general properties of the eigenfunctions by rewriting equation (16) in the Sturm-Liouville form

$$\frac{d}{dr} \left[ S(r) \frac{d\varphi_n}{dr} \right] + \lambda_n \omega(r) \varphi_n(r) = \frac{A_0 c S(r) \varphi_n(r) \delta(r - r_*)}{\kappa(r)}, \quad (17)$$

where

$$\omega(r) \equiv \frac{Su}{3\kappa} \frac{d \ln(rHu)}{dr}, \quad S(r) \equiv \frac{rH\kappa}{r_* H_* \kappa_*} \exp \left[ \frac{r_s}{\kappa_0(r_* - r_s)} - \frac{r_s}{\kappa_0(r - r_s)} \right]. \quad (18)$$

Using standard manipulations along with the asymptotic behaviors of  $S(r)$  and  $\varphi_n(r)$ , one can show that the spatial eigenfunctions form an orthogonal set. It is therefore possible to express the Green's function  $f_G$  using an expansion of the form

$$f_G(E, r) = \sum_{n=0}^{\infty} C_n \left( \frac{E}{E_0} \right)^{-\lambda_n} \varphi_n(r), \quad (19)$$

where the expansion coefficients  $C_n$  are easily computed based on the orthogonality of the eigenfunctions  $\varphi_n(r)$ .

#### 4. APPLICATION TO M87

In our numerical applications to M87, we adopt the observational values  $M \sim 3 \times 10^9 M_\odot$  (e.g., Ford et al. 1994),  $\dot{M} \sim 1.3 \times 10^{-1} M_\odot \text{ yr}^{-1}$  (Reynolds et al. 1996), and  $L_{\text{jet}} = 5.5 \times 10^{43} \text{ erg s}^{-1}$  (Reynolds et al. 1996; Bicknell & Begelman 1996; Owen, Eilek, & Kassim 2000). We utilize natural gravitational units, with  $GM = c = 1$  and  $r_s = 2$ , except as noted, and we set  $\gamma = 1.5$  (see Narayan et. al 1997). In principle, our model can accommodate any value for the viscosity parameter  $\alpha$ . We set  $\alpha = 0.1$  here in order to demonstrate that shocks can exist in ADAF disks even in the presence of substantial viscosity. The remaining parameter values implied by the observations of M87 are  $\epsilon_- = 0.001516$ ,  $\epsilon_+ = -0.005746$ ,  $j = 2.6257$ ,  $\kappa_0 = 0.01632$ ,  $\dot{N}_0 = 2.75 \times 10^{46} \text{ s}^{-1}$ ,  $\dot{N}_{\text{esc}} = 5.81 \times 10^{45} \text{ s}^{-1}$ ,  $A_0 = 0.0153$ ,  $n(r_*) = 9.52 \times 10^{43} \text{ cm}^{-3}$ ,  $U(r_*) = 8.94 \times 10^{41} \text{ erg cm}^{-3}$ ,  $E_*/E_0 = 4.70$ ,  $r_* = 26.329$ ,  $r_c^{\text{in}} = 6.462$ ,  $r_c^{\text{out}} = 96.798$ ,  $\mathcal{M}_- = 1.43$ , and  $H_* = 12.10$ . The results obtained for the inflow speed  $u$  and the isothermal sound speed  $a$  in a shocked disk are plotted in Figure 1a. The value of  $\ell$  merges with the Keplerian value  $\ell_K$  (eq. [3]) at  $r = 4,658$ , which is the outer edge of the ADAF region. Figure 1a also includes the dynamical results obtained for  $u$  and  $a$  in a smooth (shock-free) disk with  $\epsilon_- = \epsilon_+ = 0.001516$ ,  $j = 2.3988$ ,  $\kappa_0 = 0.01632$ ,  $\dot{N}_0 = 2.75 \times 10^{46} \text{ s}^{-1}$ ,  $\dot{N}_{\text{esc}} = 0$ ,  $A_0 = 0$ ,  $n(r_*) = 9.58 \times 10^{43} \text{ cm}^{-3}$ ,  $U(r_*) = 2.92 \times 10^{41} \text{ erg cm}^{-3}$ ,  $E_*/E_0 = 1.53$ ,  $r_c = 7.572$ , and  $H_* = 13.61$ . For the purposes of comparison with the shocked case, we leave the source located at  $r = 26.329$ . The value of  $j$  for the smooth solution is selected so that  $\ell = \ell_K$  at the same radius as in the shocked disk. Our results represent the first dynamical solutions for ADAF disks with isothermal shocks and a significant level of viscosity ( $\alpha = 0.1$ ). Gu & Lu (2001, 2004) obtained solutions for ADAF disks containing Rankine-Hugoniot shocks, but such shocks have conserved energy transport rates, and are therefore not relevant for producing outflows. Note that the mean energy of the relativistic particles at the source radius,  $E_*/E_0$ , is significantly larger in the shocked disk than in the smooth flow.

In Figure 1b we plot the Green's function energy distribution for the accelerated particles

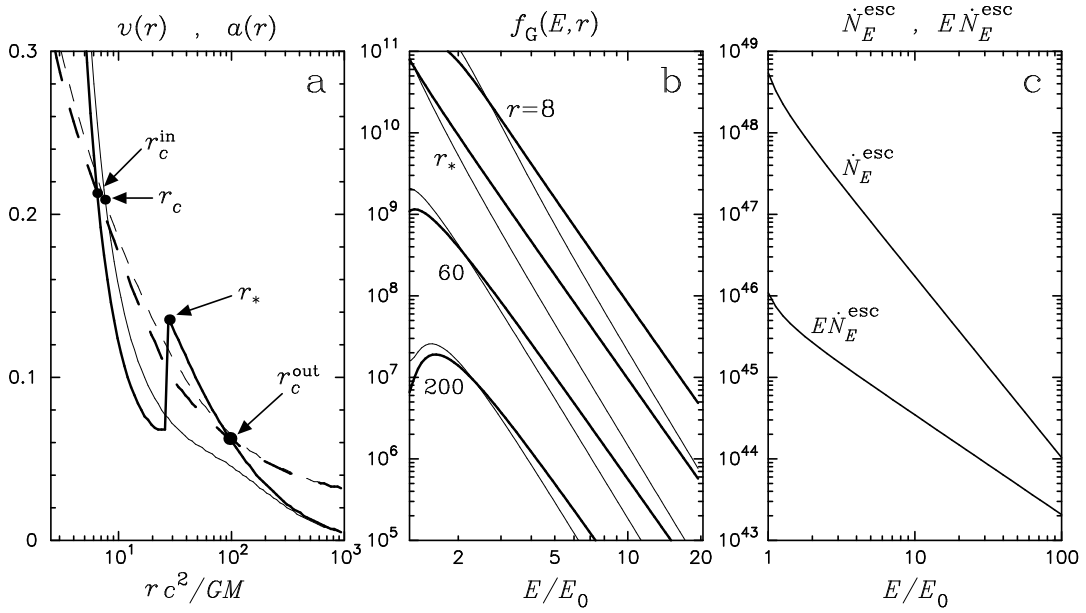


Fig. 1.— Self-consistent results for the disk structure and the particle transport obtained using the M87 parameters. (a) Inflow speed  $u(r)$  (*solid lines*) and sound speed  $a(r)$  multiplied by  $[2\gamma/(\gamma+1)]^{1/2}$  (*dashed lines*) plotted as functions of radius for shocked and smooth (shock-free) disks. (b) The Green's function particle distribution (eq. [19]) plotted as functions of energy at various radii inside the disk in cgs units. (c) The number and energy distributions for the relativistic particles escaping from the disk at the shock location (eq. [20]) plotted as a function of energy in cgs units. In panels (a) and (b), the heavy lines denote the shocked disk solutions and the thin lines represent the shock-free solutions.



measured at various radii inside the shocked and smooth disks. As expected, the presence of the shock results in a much flatter (i.e. harder) energy spectrum for the accelerated particles. In Figure 1c, we plot the number distribution  $\dot{N}_E^{\text{esc}}$  and the energy distribution  $E\dot{N}_E^{\text{esc}}$  for the particles escaping from the shocked disk, computed using (Le & Becker 2007)

$$\dot{N}_E^{\text{esc}}(E) = (4\pi E)^2 r_* H_* c A_0 f_G(E, r_*) . \quad (20)$$

The total power in the escaping particles, computed using  $L_{\text{esc}} = \int_{E_0}^{\infty} E\dot{N}_E^{\text{esc}} dE$ , is found to equal  $L_{\text{jet}} = 5.5 \times 10^{43} \text{ erg s}^{-1}$ , which is a useful self-consistency check on the model.

## 5. CONCLUSIONS

In this Letter, we have obtained for the first time dynamical solutions for viscous ADAF disks containing shocks based on a relatively large value for the standard Shakura-Sunyaev viscosity parameter,  $\alpha = 0.1$ . Utilizing a rigorous mathematical approach, we have computed the Green's function energy distribution for the relativistic particles accelerated in the disk, for both shocked and smooth disks. The results confirm that viscous disks with shocks are much more efficient particle accelerators than smooth disks. We conclude that the presence of a shock is an essential ingredient in the formation of the observed outflows. The absence of strong outflows from luminous X-ray sources probably reflects the fact that the gas is too dense to allow efficient Fermi acceleration of a relativistic particle population in the disk. This helps to explain the observed anticorrelation between X-ray luminosity and radio/outflow strength (e.g., Reynolds et al. 1996). Our results establish that the luminosity of the M87 jet can be understood within the context of the disk/shock/outflow model. However, collimation effects and radiative losses must also be considered in order to understand the subsequent propagation of the jet through the extragalactic environment.

## REFERENCES

- Abramowicz, M. A. & Chakrabarti, S. K. 1990, ApJ, 350, 281
- Becker, P. A., Le, T. 2003, ApJ, 588, 408
- Bicknell, G. V., & Begelman, M. C. 1996, ApJ, 467, 597
- Chakrabarti, S. K. 1989, Publ. Astron. Soc. Japan, 41, 1145
- Ford, H. C. et al. 1994, ApJ, 435, L27

- Frank, J., King, A. R., & Raine, D. J. 2002, *Accretion Power in Astrophysics* (Cambridge: Cambridge University Press)
- Gu, W.-M., & Lu, J.-F. 2001, *Chin. Phys. Lett.*, 18, 148
- Gu, W.-M., & Lu, J.-F. 2004, *Chin. Phys. Lett.*, 21, 2551
- Le, T., & Becker, P. A. 2004, *ApJ*, 617, L25
- Le, T., & Becker, P. A. 2005, *ApJ*, 632, 476
- Le, T., & Becker, P. A. 2007, *ApJ*, 661, 416
- Lu, J.-F., Gu, W.-M., & Yuan, F. 1999, *ApJ*, 523, 340
- Narayan, R., Kato, S., & Honma, F. 1997, *ApJ*, 476, 49
- Owen, F. N., Eilek, J. A., & Kassim, N. E. 2000, *ApJ*, 543, 611
- Paczynski, B., & Wiita, P. J. 1980, *A&A*, 88, 23
- Reynolds, C. S. et al. 1996, *MNRAS*, 283, L111
- Shakura, N. I., & Sunyaev, R. A. 1973, *A&A*, 24, 337